Article

Current Biology

Single-Cell Transcriptomes Reveal Diverse Regulatory Strategies for Olfactory Receptor Expression and Axon Targeting

Graphical Abstract

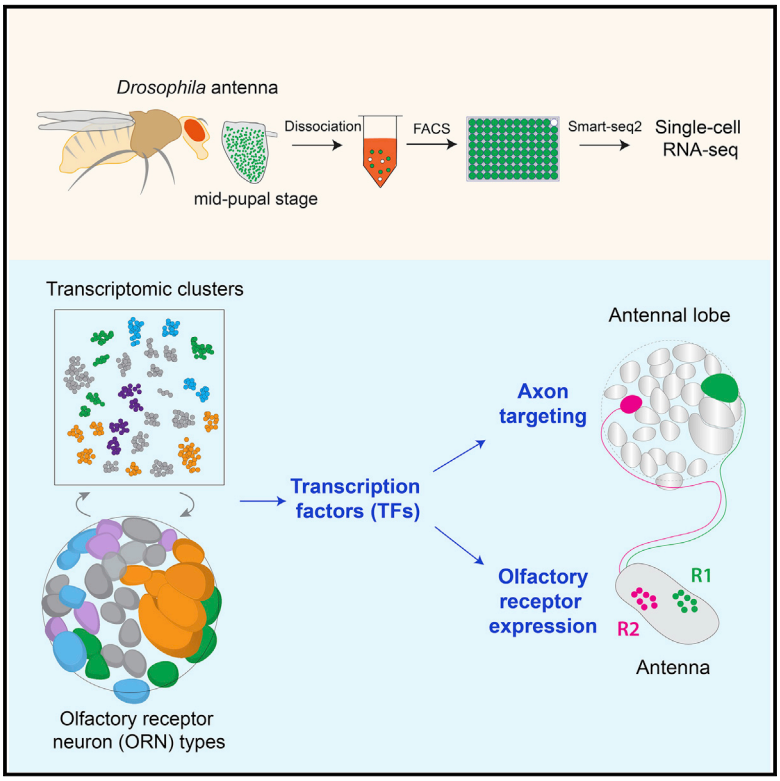

Highlights

- Single-cell RNA-seq analysis of developing *Drosophila* olfactory receptor neurons
- 20 of the 33 transcriptomic clusters of ORNs are mapped to glomerular types
- Each ORN type expresses hundreds of transcription factors (TFs)
- Homeodomain TF Unpg regulates both olfactory receptor expression and axon targeting

Authors

Hongjie Li, Tongchao Li, Felix Horns, ..., David J. Luginbuhl, Stephen R. Quake, Liqun Luo

Correspondence

hongjie@stanford.edu (H.L.), quake@stanford.edu (S.R.Q.), lluo@stanford.edu (L.L.)

In Brief

In this study, Li et al. perform single-cell RNA sequencing of developing olfactory receptor neurons (ORNs) in *Drosophila* and reveal that ORNs utilize diverse transcriptional strategies to coordinate their olfactory receptor expression and axon targeting.

Li et al., 2020, Current Biology *30*, 1189–1198
April 6, 2020
https://doi.org/10.1016/j.cub.2020.01.049

CellPress

Current Biology
Article

Single-Cell Transcriptomes Reveal Diverse Regulatory Strategies for Olfactory Receptor Expression and Axon Targeting

Hongjie Li,[1,6,*] Tongchao Li,[1,6] Felix Horns,[2,4] Jiefu Li,[1] Qijing Xie,[1,3] Chuanyun Xu,[1] Bing Wu,[1] Justus M. Kebschull,[1] Colleen N. McLaughlin,[1] Sai Saroja Kolluru,[4] Robert C. Jones,[4] David Vacek,[1] Anthony Xie,[1] David J. Luginbuhl,[1] Stephen R. Quake,[4,5,*] and Liqun Luo[1,7,*]

[1]Department of Biology and Howard Hughes Medical Institute, Stanford University, Stanford, CA 94305, USA
[2]Biophysics Graduate Program, Stanford University, Stanford, CA 94305, USA
[3]Neurosciences Graduate Program, Stanford University, Stanford, CA 94305, USA
[4]Department of Bioengineering and Department of Applied Physics, Stanford University, Stanford, CA 94305, USA
[5]Chan Zuckerberg Biohub, Stanford, CA 94305, USA
[6]These authors contributed equally
[7]Lead Contact
*Correspondence: hongjie@stanford.edu (H.L.), quake@stanford.edu (S.R.Q.), lluo@stanford.edu (L.L.)
https://doi.org/10.1016/j.cub.2020.01.049

SUMMARY

The regulatory mechanisms by which neurons coordinate their physiology and connectivity are not well understood. The *Drosophila* olfactory receptor neurons (ORNs) provide an excellent system to investigate this question. Each ORN type expresses a unique olfactory receptor, or a combination thereof, and sends their axons to a stereotyped glomerulus. Using single-cell RNA sequencing, we identified 33 transcriptomic clusters for ORNs and mapped 20 to their glomerular types, demonstrating that transcriptomic clusters correspond well with anatomically and physiologically defined ORN types. Each ORN type expresses hundreds of transcription factors. Transcriptome-instructed genetic analyses revealed that (1) one broadly expressed transcription factor (Acj6) only regulates olfactory receptor expression in one ORN type and only wiring specificity in another type, (2) one type-restricted transcription factor (Forkhead) only regulates receptor expression, and (3) another type-restricted transcription factor (Unplugged) regulates both events. Thus, ORNs utilize diverse strategies and complex regulatory networks to coordinate their physiology and connectivity.

INTRODUCTION

The ultimate function of a neuron is determined by both its physiology and connectivity, but the transcriptional regulatory mechanisms that coordinate these two features are not well understood [1–4]. In the *Drosophila* adult olfactory system, there are 50 types of olfactory receptor neurons (ORNs). Each ORN type expresses a single olfactory receptor, or a unique combination thereof, which determines its physiological reponses to olfactory stimuli. Each ORN type also sends axons to a stereotyped glomerulus, which determines how the olfactory signal is represented in the brain [5–9]. The mammalian olfactory system shares these two features [10]. In mice, the coordination of olfactory receptor expression and wiring specificity is accomplished in part by olfactory receptors themselves regulating ORN wiring specificity [11–13]. However, *Drosophila* olfactory receptors do not regulate axon targeting [5, 14], raising the question of how receptor expression and wiring specificity are coordinated.

Single-cell RNA sequencing (scRNA-seq) has been used to classify neurons and identify markers in diverse organisms and brain regions [e.g., 15–21]. Determining single-cell transcriptomes should also facilitate the investigation of mechanisms that regulate olfactory receptor expression and axon targeting. Here, we performed scRNA-seq for fly antennal ORNs and identified 33 distinct transcriptomic clusters. We unambiguously mapped 20 clusters to their glomerular types, demonstrating that transcriptomic clusters correspond well with anatomically and physiologically defined ORN types. To understand transcriptional regulation of receptor expression and wiring, we comprehensively analyzed the expression patterns of all detected transcription factors (TFs) from our sequenced cells and found that each ORN cluster expresses hundreds of TFs. We then performed a targeted genetic screen focusing on TFs that are restricted to only a few clusters and identified the TF *unpg* that regulates both olfactory receptor expression and wiring, two fundamental features of sensory neurons. Together with genetic analysis of two other TFs, our findings revealed that ORNs utilize diverse transcriptional regulatory strategies to coordinate olfactory receptor expression and axon targeting.

RESULTS

scRNA-Seq of Developing *Drosophila* ORNs

To identify molecular mechanisms underlying olfactory receptor expression and axon targeting, we first profiled transcriptomes of single ORNs from the *Drosophila* antenna at 42–48 h after puparium formation (hereafter termed 48hAPF). Transcriptomic

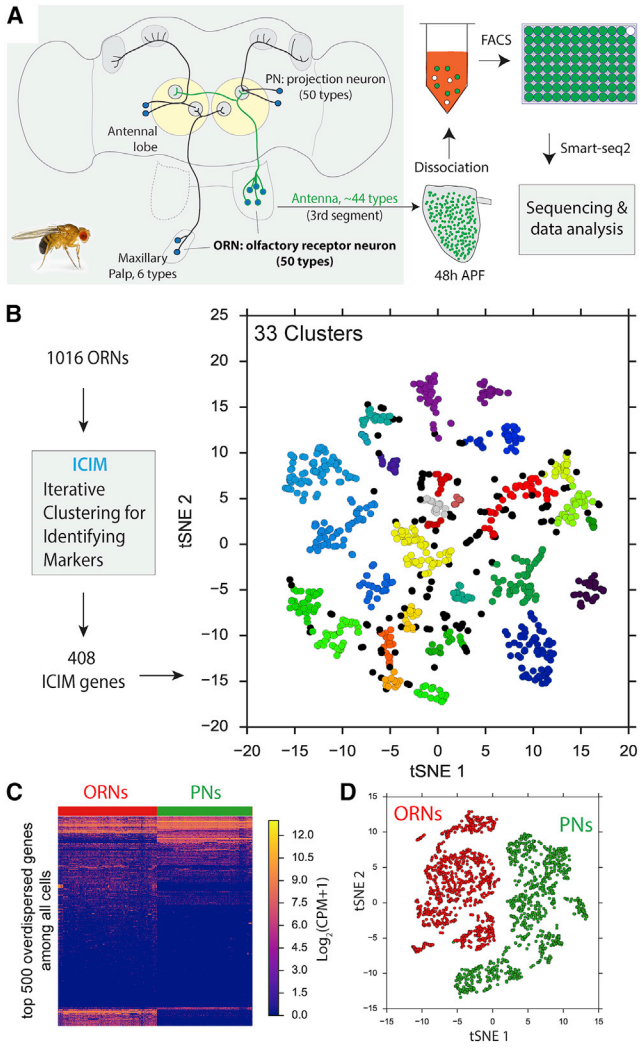

Figure 1. Single-Cell RNA-Seq of *Drosophila* Olfactory Receptor Neurons (ORNs) at 48hAPF.

(A) Schematic of the fly olfactory system and scRNA-seq workflow. 50 ORN types (44 from the third segment of the antenna and 6 from the maxillary palp) send axons to the antennal lobe to form stereotypical one-to-one connections with 50 types of projection neurons (PNs). The third segments of pupal antennae were manually dissected, GFP+ ORNs were sorted into 96-well plates using fluorescence-activated cell sorting (FACS), and the Smart-seq2 protocol was used for library preparation and sequencing [23].

(B) Visualization of ORN transcriptomic clusters using t-distributed stochastic neighbor embedding (tSNE) plot based on 408 genes identified by iterative clustering for identifying markers (ICIM). Each dot indicates a cell. 1,016 ORNs at 48hAPF (908 from pan-ORN *nSyb-GAL4*, 63 from *85A10-GAL4*, and 45 from *AM29-GAL4*) form 33 distinct clusters. Black dots indicate cells that could not be assigned to any cluster.

(C) Hierarchical heatmap showing clear separation of 1,016 ORNs (red) and 946 PNs (green) using the top 500 overdispersed genes identified across all cells. Each column indicates one cell, and each row indicates one gene. ORNs are from 48hAPF. PNs are from 24hAPF [19]. Expression levels are indicated by the color bar (CPM, counts per million sequencing reads). Cells (columns) and genes (rows) are ordered using hierarchical clustering.

(D) Visualization of ORNs (red) and PNs (green) using principal-component analysis followed by tSNE plot using top 500 overdispersed genes.

See also Figure S1.

analysis at this stage will allow us to capture molecules regulating both of these two events, because ORNs are completing their axon targeting [22] and olfactory receptors begin to express at 48hAPF [5, 7, 14]. Using plate-based scRNA-seq with SMART-seq2 [19, 23], we obtained 1,016 high-quality cells from about 44 types of antennal ORNs, with each cell sequenced to a depth of ~1 million reads resulting in ~1,500 detected genes (Figure 1A; Figures S1A–S1C; STAR Methods). Using an unsupervised machine-learning algorithm [19] and hierarchical density-based unbiased clustering [24], we identified 33 distinct transcriptomic clusters (Figure 1B; Figures S1D–S1F).

Drosophila ORNs and projection neurons (PNs) are synaptic partners in the antennal lobe. We compared their transcriptomic differences using the 1,016 ORNs here with 946 PNs sequenced previously [19]. Using either highly variable genes across all ORNs and PNs or differentially expressed genes between them, ORNs and PNs were readily separated into two distinct groups (Figures 1C and 1D; Figure S1G). We further identified several ORN- and PN-specific genes, including widely used ORN and PN markers (Figure S1H), and validated the expression of a newly identified ORN-specific gene [25] (Figure S1I).

Matching Transcriptomic Clusters with Glomerular Types

We next used three strategies to map transcriptomic clusters to anatomically and functionally defined ORN types. First, we used *AM29-GAL4* [26]- and *85A10-GAL4* [27]-driven GFP expression to label two and five distinct ORN types, respectively, and sequenced these cells at 48hAPF (Figure 2A). As expected, *AM29*+ and *85A10*+ ORNs mapped to two and five distinct ORN clusters, respectively (Figure 2B; Figures S2C and S2I). Second, we used the expression of *fruitless* (*fru*) in three ORN types [28] to define three more clusters (Figure S2M).

Third, we used olfactory receptor expression to map transcriptomic clusters to glomerular types based on previously established correspondence between olfactory receptor expression and glomerular targets [8, 29–31]. We first systematically assessed the expression of olfactory receptors, including all chemosensory receptors in the olfactory system belonging to the Or (odorant receptor), Gr (gustatory receptor), and Ir (ionotropic receptor) families [5, 7, 32, 33]. Excluding co-receptors expressed in multiple adult ORN types (*Orco* and *Ir25a*, which act in concert with type-specific receptors for odor detection) [31, 34], we found that 37% of ORNs expressed olfactory receptors at 48hAPF (Figure 2C), consistent with the previous finding that olfactory receptors are gradually turned on during pupal development [7]. We then used detected receptors to futher assign positive clusters to specific glomerular types (Figures S2A, S2B, S2D–S2H, S2J–S2L, and S2N–S2U).

The three strategies gave congruent results when mapping the same clusters and allowed us to decode the glomerular identity of 18 clusters in total. We further validated our cluster identity assignments using *GAL4* drivers from specific genes. In all cases, the GAL4 expression patterns matched their cluster identities (Figures 2D and 2E; Figures S2V–S2Y), suggesting robust mapping between transcriptomic clusters and glomerular types. The only exception to the one-to-one matching between transcriptomic clusters and glomerular types is that cluster 9

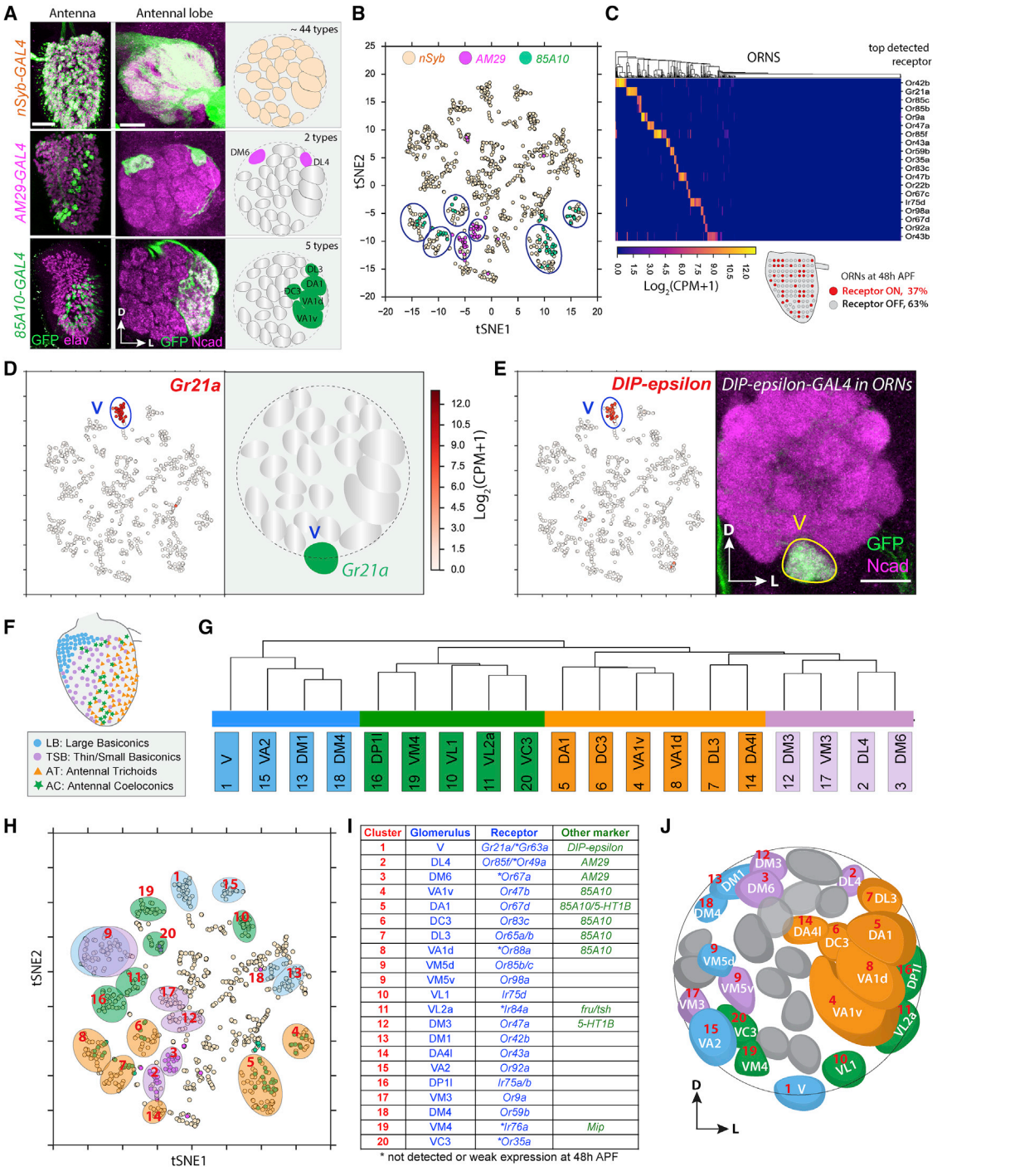

Cluster	Glomerulus	Receptor	Other marker
1	V	*Gr21a/*Gr63a*	*DIP-epsilon*
2	DL4	*Or85f/*Or49a*	*AM29*
3	DM6	**Or67a*	*AM29*
4	VA1v	*Or47b*	*85A10*
5	DA1	*Or67d*	*85A10/5-HT1B*
6	DC3	*Or83c*	*85A10*
7	DL3	*Or65a/b*	*85A10*
8	VA1d	**Or88a*	*85A10*
9	VM5d	*Or85b/c*	
9	VM5v	*Or98a*	
10	VL1	*Ir75d*	
11	VL2a	**Ir84a*	*fru/tsh*
12	DM3	*Or47a*	*5-HT1B*
13	DM1	*Or42b*	
14	DA4l	*Or43a*	
15	VA2	*Or92a*	
16	DP1l	*Ir75a/b*	
17	VM3	*Or9a*	
18	DM4	*Or59b*	
19	VM4	**Ir76a*	*Mip*
20	VC3	**Or35a*	

* not detected or weak expression at 48h APF

Figure 2. Mapping Transcriptomic Clusters to Glomerular Types

(A) Three drivers were used to label ORNs for scRNA-seq: *nSyb-GAL4* for all ORNs and *AM29-GAL4* and *85A10-GAL4* for two and five specific ORN types, respectively. Confocal images show the expression patterns of these drivers in both antenna and antennal lobe at 48hAPF. All drivers were crossed with *ey-Flp;UAS-FRT-STOP-FRT-mCD8:GFP* to restrict the GFP expression to cells in the antenna. Elav staining labels neuronal nuclei, and N-cadherin (NCad) staining labels neuropil.

(B) Visualization of *nSyb+*, *AM29+*, and *85A10+* ORNs using a tSNE plot as in Figure 1B. Cells are colored according to drivers. *AM29+* cells (magenta) map to two clusters, and *85A10+* cells (green) map to five clusters (circled). Note that several individual cells from both drivers fall into other clusters, likely due to stochastic sparse labeling of these two drivers in other ORNs beyond the seven ORN types.

(C) Heatmaps showing the top 19 detected olfactory receptor genes in 1,016 ORNs. Each column indicates an individual ORN from 48hAPF. Cells are ordered using hierarchical clustering.

(D) tSNE plots showing *Gr21a* expression. *Gr21a+* ORNs target axons to glomerulus V.

(legend continued on next page)

corresponds to two ORN types, VM5d and VM5v (Figures S2J and S2K).

Relationship between Transcriptomes, Lineage, and Spatial Patterning

Each antennal ORN is housed in one of four types of sensory organs called sensilla. Each sensillum contains 1–4 ORNs derived from a common progenitor, with a stereotyped combination of ORN type, morphology, and spatial distribution [8, 29] (Figure 2F; Figure S3A). To examine the relationship between transcriptomes, lineage, and spatial patterning of antennal ORNs, we compared transcriptomes that we had mapped to the glomerular types. We found that ORNs that belong to the same sensillar type (large basiconics, small basiconics, tricoids, or coeloconics) share more similar transcriptomes compared to ORNs that belong to different sensillar types (Figure 2G; Figures S3B and S3C), based on our decoded clusters. We also note two exceptions: two clusters (DL3 and DA4l) from antennal tricoides are more similar to thin and small basiconics ORNs from our hierarchical clustering analysis (Figure 2G; Figure S3C). ORNs within the same sensillum did not exhibit additional similarities when compared to ORNs that were from the same sensillar types yet from different sensilla (Figure S3D). We further identified differentially expressed genes between four sensillar types and noticed that TFs and cell-surface molecules (CSMs) account for a large proportion (Figures S4A–S4C), suggesting a critical role for these two sets of genes during this developmental stage.

These analyses suggest that spatial distributions across the antenna, which separate different sensillar types (Figure 2F), are an important determinant for transcriptomes of individual ORN types. We predicted the sensillar types of two previously unidentified transcriptomic clusters based on hierarchical clustering (Figure 2G) and validated the identity of their corresponding glomeruli with experimental data (Figures S3E–S3H).

In summary, we mapped a total of 20 transcriptomic clusters to 21 specific glomerular types (Figures 2H–2J), establishing a nearly one-to-one correspondence between transcriptomic clusters and anatomically and physiologically defined ORN types. Our annotated dataset provides a valuable resource for studying the development and function of individual ORN types.

TF Expression Analyses in ORNs

We next investigated the mechanisms by which TFs regulate olfactory receptor expression and wiring specificity. In principle, three types of TFs may exist: those that regulate wiring specificity only, receptor expression only, or both (Figure 3A). We first compared expression levels between TFs and other genes in the genome. Contrary to the notion that TFs are usually expressed at relatively low levels [35], we found no significant differences between the expression levels of TFs and non-TFs in the genome (Figure 3B).

We next characterized TF expression at the level of cells and clusters with the following criteria: a positive cluster is defined as more than 30% cells in the cluster expressing the TF at the level of $\log_2(\text{CPM} + 1) \geq 3$, where CPM represents transcript counts per million. Of the 1,045 TFs in the fly genome [36], 899 were expressed in at least one ORN, and, on average, about 150 TFs were detected in individual ORNs (Figure 3C). At the cluster level, 423 TFs were detected in one or more clusters, exhibiting a wide range of expression patterns (Figures 3D and 3E). Next, we sought to identify TFs that regulate olfactory receptor expression and wiring specificity based on our transcriptomic data.

POU-Domain TF Acj6 Regulates Olfactory Receptor Expression in One ORN Type but Axon Targeting in Another

Previous studies have identified several TFs that regulate *Drosophila* olfactory receptor expression or wiring specificity [5, 37–41]. However, with the exception of one study on ORN fate diversification [26], these two processes have been investigated separately within the same ORN type because of a lack of appropriate genetic tools. Transgenes utilizing olfactory receptor promoter-driven GFP were used to visualize ORN axon targeting in most cases. If a TF were required for olfactory receptor expression, deleting the TF would lead to the loss of olfactory receptor expression, so that ORN axon targeting could not be visualized. We overcame this obstacle by using a GAL4 reporter whose expression is independent of olfactory receptors, as well as additional methods (discussed later).

We first analyzed a POU-domain TF, *abnormal chemosensory jump 6* (*acj6*), which is expressed in most antennal ORNs and regulates receptor expression in some ORN types and axon targeting in other ORN types [37, 38, 41]. However, it is unclear whether *acj6* regulates both wiring specificity and receptor expression in the same ORN type. Our sequencing data showed that *acj6* was expressed in all ORN clusters, including those that express *AM29-GAL4* and target axons to the DL4 and DM6 glomeruli (hereafter termed DL4-ORNs and DM6-ORNs) (Figures 3E and 4A). Using an *acj6* null allele [37], we found that *acj6* was required for the expression of *Or85f* in DL4-ORNs but not required for the expression of *Or67a* in DM6-ORNs (Figure 4A), consistent with previous results [41]. Using *AM29-GAL4* to independently label the axons of DL4- and DM6-ORNs, we found that DM6-ORNs showed highly penetrant mistargeting phenotypes, while DL4-ORNs still targeted to the correct glomerulus (Figure 4A). To test whether *acj6* regulates the axon targeting cell autonomously, we performed a mosaic analysis with a repressible cell marker (MARCM), where homozygous mutant cells are

(E) Validation of the decoded cluster. Intersecting *ey-Flp* with *DIP-epsilon-T2A-GAL4* specifically labels V-ORNs (GFP, green) at 48hAPF. N-cadherin (NCad) staining labels neuropil.
(F) Spatial distribution of ORNs from four sensillar groups in the antenna; adapted from [29], with permission.
(G) Hierarchical clustering of ORNs based on the heatmap in Figure S3C. Sensillar groups are colored according to the key in (F).
(H–J) Summary of 20 transcriptomic clusters (H) that have been mapped to 21 glomerular types with their names and corresponding markers (I) and with their maps in the antennal lobe (J). Note that cluster 9 was mapped to two ORN types, VM5d and VM5v.
D, dorsal; L, lateral. Scale bars, 20 μm.
See also Figures S2, S3, and S4.

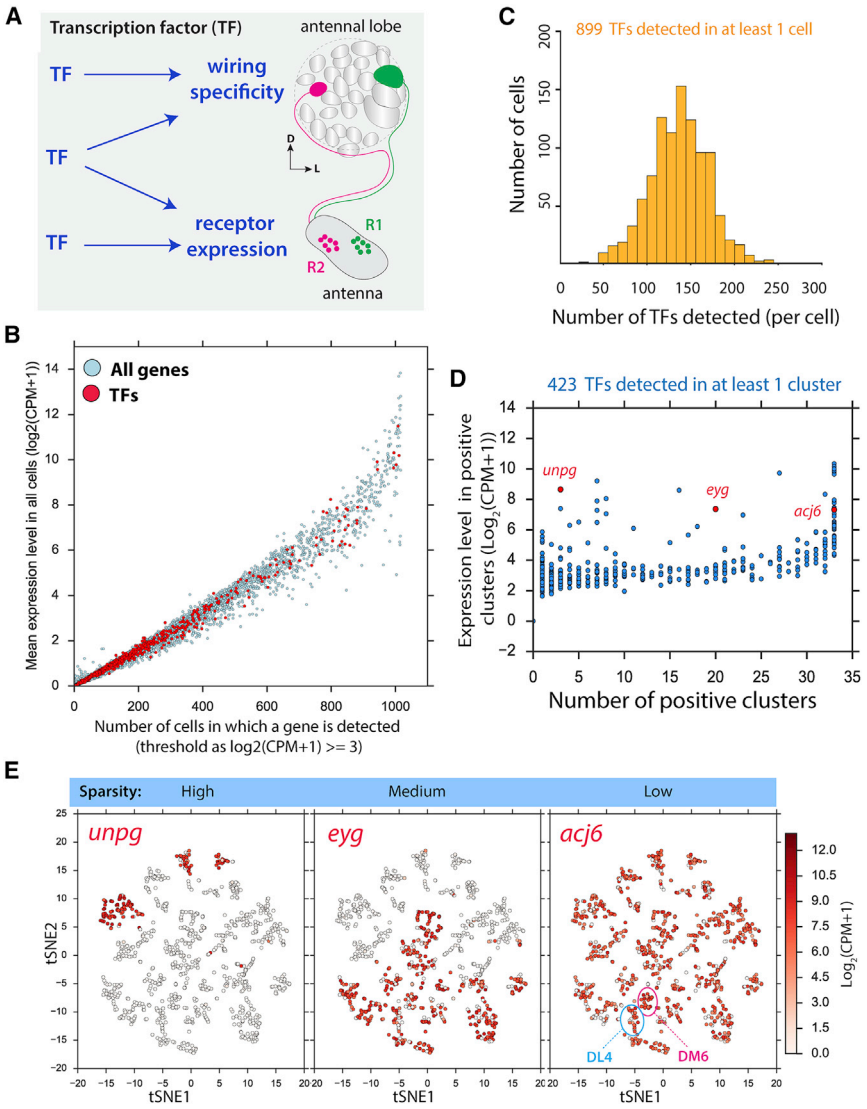

Figure 3. TF Expression in ORNs

(A) Schematic showing three kinds of TFs that regulate olfactory receptor expression and wiring specificity.

(B) Scatterplots showing number of cells in which a gene can be detected versus the mean expression level of the gene in all cells. TFs are highlighted. A positive cell is defined as the cell expressing a gene at the level of $\log_2(\text{CPM} + 1) \geq 3$. CPM, counts per million. This analysis shows that TFs have a wide range of expression patterns, from a few cells or all cells, and that the overall TF expression level is comparable with other types of genes.

(C) Distributions of the number of TFs detected per ORN at the level of $\log_2(\text{CPM} + 1) \geq 3$.

(D) Sparsity and expression level of the TFs among ORN transcriptomic clusters. Each dot indicates one TF. A positive cluster is defined as more than 30% cells in the cluster expressing the TF at the level of $\log_2(\text{CPM} + 1) \geq 3$. Highlighted in red are three example genes, *unpg*, *eyg*, and *acj6*, with high mean expression levels but different sparsity.

(E) tSNE plots showing expression of *unpg*, *eyg*, and *acj6*. Expression levels are indicated by the color bar. In the *acj6* tSNE plot, two clusters corresponding to DL4 and DM6 are indicated. Feature maps like those shown in (E) can be produced for any of the TFs listed in (D) with the transcriptomic data that we have deposited in Github.

labeled within an otherwise mostly heterozygous genetic background [42]. Sparse MARCM clones visualized by *AM29-GAL4* revealed similar mistargeting of DM6-ORNs but normal targeting of DL4-ORNs (Figure 4B). These experiments suggest that *acj6* acts cell autonomously to regulate axon targeting of DM6-ORNs but not DL4-ORNs. In summary, *acj6* is required for wiring but not receptor expression in DM6-ORNs and is required for receptor expression but not wiring in DL4-ORNs (Figure 4C).

Homeodomain TF Unplugged Regulates Both Olfactory Receptor Expression and ORN Axon Targeting

To test whether type-restricted TF expression also contributes to olfactory receptor expression and wiring specificity, we focused on ORNs targeting to glomerulus V (hereafter termed V-ORNs), which co-express two olfactory receptors, *Gr21a* and *Gr63a* [43, 44]. We performed an RNAi screen on 25 candidate TFs expressed in only a few transcriptomic clusters, including V-ORNs. This screen identified two TFs. The first TF is the founding member of the FOX family of TFs, Forkhead (Fkh) [45], which is expressed in two clusters, including V-ORNs (Figure 5A). Knockdown of *fkh* drastically reduced the reporter expression for both *Gr21a* and *Gr63a* (Figure 5B). However, the size and shape of the V glomerulus and axon targeting reflected by residual reporter expression appeared normal (Figure 5B), suggesting that *fkh* is required for normal receptor expression but not for wiring of V-ORNs.

The second TF is the homeobox TF Unplugged (Unpg), previously identified as a regulator of tracheal branch formation [46] and as a marker for a specific neuroblast sub-lineage [47]. We found *unpg* expression in three transcriptomic clusters mapped to four ORN types: V (*Gr21a*/*Gr63a*+), VA2 (*Or92a*+), VM5d (*Or85b*+), and VM5v (*Or98a*+) (Figures 5C and 5D). Because the *Or85b* reporter was barely detectable in control flies, we focused our subsequent analysis on the other three ORN types. We found that RNAi knockdown of *unpg* in ORNs caused loss of receptor expression in all three *unpg*+ ORN types but not in four *unpg*− ORN types (Figures 5E and 5F; Figures S5A–S5C), suggesting that *unpg* is specifically required for olfactory receptor expression in *unpg*+ ORNs. Since two *unpg*− ORNs were from the same sensilla as *unpg*+ ORNs that express *Or92a* and *Gr21a* (Figure 5H), these data suggest that the loss of *Or92a* and *Gr21a* in *unpg-RNAi* flies was not due to gross developmental defects of the sensilla.

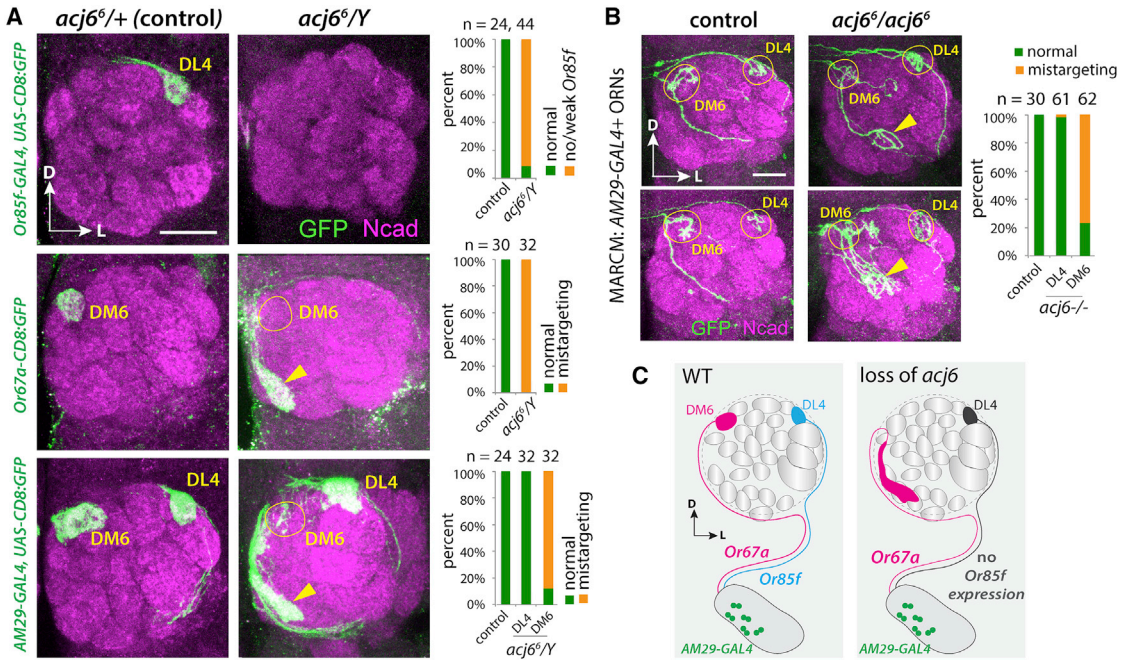

Figure 4. Role of *acj6* in Olfactory Receptor Expression and Axon Targeting

(A) Confocal images of adult antennal lobes showing ORN axon targeting in heterozygous control (left) and hemizygous mutant (right). In *acj6* mutants, *Or85f* expression is lost, but DL4 ORN axons still target normally as shown by *AM29-GAL4*; *Or67a* expression is normal, but DM6 ORN axons mistarget (arrowhead in the middle), as confirmed by *AM29-GAL4* (arrowhead on the bottom).

(B) Sparse MARCM clones visualized by *AM29-GAL4* revealed mistargeting of ORN axons that took the medial trajectory, with a mistargeting phenotype (arrowheads) highly similar to mistargeting of DM6-ORN axons labeled by *Or67a* in *acj6* mutant (Figure 3F). ORN axons that took the lateral trajectory targeted normally to the DL4 glomerulus. Quantifications are shown on the right, with antennal lobe numbers (n) on top.

(C) Schematic summary: *acj6* is required for receptor expression but not for wiring specificity in DL4-ORNs and is required for wiring specificity but not for receptor expression in DM6-ORNs. All confocal images are z stacks covering the region of target glomeruli. N-cadherin (NCad) staining labels neuropil.

D, dorsal; L, lateral; WT, wild type. Scale bars, 20 μm.

Does *unpg* also regulate axon targeting? Interestingly, unlike *Gr21a* in V-ORNs, the co-expressed receptor *Gr63a* was not downregulated by *unpg* RNAi knockdown, and *Gr63a*+ axons showed stereotyped mistargeting in all *unpg-RNAi* flies (Figure 5G). The V glomerulus was also smaller and misshapen, likely reflecting a lack of proper V-ORN axon targeting. Thus, *unpg* regulates both *Gr21a* expression and axon targeting of V-ORNs. We note that some V-ORN axons in *unpg-RNAi* flies still targeted to the correct glomerulus. This is consistent with previous studies where deleting a single gene usually leads to partial mis-wiring phenotypes, presumably due to partial redundancy of regulators of wiring specificity [19, 48].

Two additional approaches using PN dendrite targeting and DiI labeling of ORN axons revealed that *unpg* also controls axon targeting in three other *unpg*+ ORN types: VM5d, VM5v, and VA2 (Figures 5H and 5I; Figure S5D). We identified a Janelia-GAL4 driver [27], *GMR86C10-GAL4*, that specifically labels VM5d and VM5v PNs and generated a *GMR86C10-LexA* driver to label these PNs independent of the GAL4/UAS system. Since ORN axon mistargeting during development can lead to dendrite mistargeting of partner PNs [49, 50], we reasoned that we might observe mistargeting of VM5d and VM5v PNs if knocking down *unpg* in VM5d and VM5v ORNs causes targeting defects. This was, indeed, the case (Figure S5D), as we observed that VM5d and VM5v PN dendrites showed mistargeting phenotypes when *unpg* was only knocked down in ORNs using pan-ORN *peb-GAL4*. This result suggests that *unpg* also regulates VM5d and VM5v ORN axon targeting.

Finally, we utilized the fluorescent lipophilic DiI-mediated anterograde tracing to examine axon targeting of *Or92*+ VA2-ORNs. Each ab1 sensillum houses four ORNs: two are *unpg*−, and two are *unpg*+ (V-ORNs and VA2-ORNs; Figure 5H) [29]. By applying DiI to a small subset of ab1 sensilla to initiate anterograde tracing, we found that two *unpg*− ORN types targeted their axons normally as expected, while the two *unpg*+ ones showed stereotyped mistargeting (Figure 5I), suggesting that *unpg* also regulates axon targeting of VA2-ORNs. Taken together, our data suggest that *unpg* controls both olfactory receptor expression and wiring specificity within the same ORN types (Figure 5J; Figure S5E).

DISCUSSION

Using plate-based scRNA-seq, we analyzed high-quality transcriptomes of 1,016 antennal ORNs at a mid-pupal stage, when ORNs are completing their axon targeting to their cognate glomeruli and a subset of ORNs start to express olfactory receptors. The smaller number of transcriptomic clusters (33) compared to glomerular types (44 for antennal ORNs) may result from the following: (1) for some ORN types, not enough cells

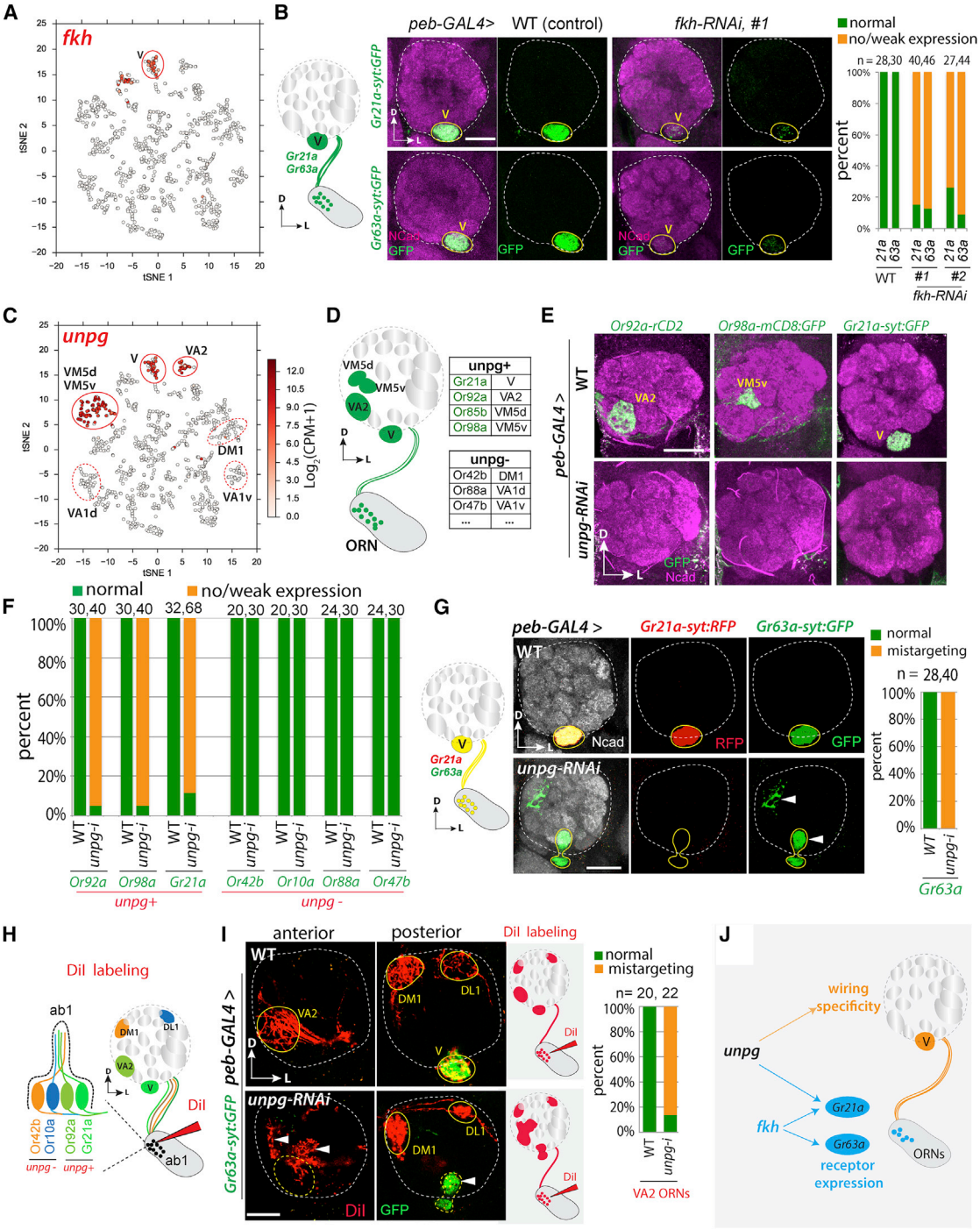

Figure 5. Transcriptional Control of Olfactory Receptor Expression and Wiring Specificity in V-ORNs

(A) tSNE plot showing that *fkh* is expressed in two clusters, one of which corresponds to V-ORNs.

(B) Olfactory receptors *Gr63a* and *Gr21a* are co-expressed in V-ORNs. Confocal images of adult antennal lobes show that ORN knockdown of *fkh* using *peb-GAL4;UAS-dcr2* causes markedly reduced expression of markers driven from transgenes utilizing the promoters of *Gr21* and *Gr63*; quantified on the right with antennal lobe number (n) on top. Residual marker expression indicates that *Gr21a*/*Gr63a*+ axons still target to V.

(C) tSNE plot showing that *unpg* is expressed in three clusters mapped to V, VA2, and VM5d/VM5v (solid outline). Three *unpg*− clusters are indicated (dashed outline).

(D) Schematic summarizing receptor expression and glomerular targets of all *unpg*+ and some *unpg*− ORN types.

(E) Confocal images of adult antennal lobes showing olfactory receptor expression in control (WT) and *unpg-RNAi* flies. *peb-GAL4;UAS-dcr2* was crossed with either w^{1118} (WT) or *unpg-RNAi*, and olfactory receptor promoter-driven reporters were used to monitor receptor expression. In WT flies, *Or92a*, *Or98a*, and *Gr21a* are expressed normally. In *unpg-RNAi* flies, the expression of all three receptors is lost.

(legend continued on next page)

were captured to reach the minimal requirement of forming a cluster (see STAR Methods for criteria for transcriptomic clusters); and (2) closely related ORN types may form one transcriptomic cluster (e.g., cluster 9 corresponds to two ORN types, VM5d and VM5v; Figures S2J and S2K). Besides olfactory receptor neurons, there are also other sensory cells in the third segment of the antenna; for example, hygro- and thermo-sensory neurons in the sacculus and arista. It has been shown that all those neurons express *Ir25a* and *Ir93a*, and different subsets express *Ir21a*, *Ir40a*, *Ir68a*, and *Gr28b* in adult flies [33, 51–54]. Our scRNA-seq data show that *Ir25a* is broadly expressed in many ORN types, but all other aforementioned genes are not expressed at 48hAPF. Due to the lack of specific markers, we could not define these cells. Compared to the large number of ORNs, these other cells likely constitute a minority of cells.

Our understanding of how developing neurons coordinately regulate physiological properties and connectivity is limited to only a few examples [11–13, 55, 56]. Here, we found that even in the same group of neurons (*Drosophila* ORNs), the coordination of these two features uses diverse transcriptional strategies. On one hand, the broadly expressed *acj6* regulates receptor expression but not wiring in one ORN type and wiring but not receptor expression in a second type. On the other hand, the type-restricted *unpg* regulates both receptor expression and wiring specificity in all ORN types that express *unpg* (Figure S5E). However, within the V-ORNs, the type-restricted *fkh* regulates the expression of both co-receptors, but not wiring, whereas *unpg* regulates only one of the two co-receptors, arguing against a simple regulatory relationship (Figure 5J). The complexity of the regulatory network inferred from our study is, perhaps, a result of the evolution of different ORN types in a piecemeal fashion, as reflected by their utilizing three distinct families of chemoreceptors as olfactory receptors [5–7, 33, 34]. Untangling this complexity requires future studies to systematically identify transcriptional targets of these TFs and investigate their regulatory relationship.

In conclusion, scRNA-seq in developing *Drosophila* ORNs enabled us to map 20 transcriptomic clusters to glomerular types. This reinforces the idea that neuronal transcriptomic identity corresponds well with anatomical and physiological identities defined by connectivity and function in well-defined neuronal types [17, 19]. Our genetic analyses further suggest that ORNs utilize diverse regulatory strategies to coordinate their physiology and connectivity. Given that each ORN type expresses hundreds of TFs, it is remarkable that the loss of a single TF, *unpg*, can result in profound disruption of receptor expression and wiring specificity, two most fundamental properties of sensory neurons.

STAR★METHODS

Detailed methods are provided in the online version of this paper and include the following:

- KEY RESOURCES TABLE
- LEAD CONTACT AND MATERIALS AVAILABILITY
- EXPERIMENTAL MODEL AND SUBJECT DETAILS
  - Fly stocks
- METHOD DETAILS
  - Immunostaining
  - MARCM analysis
  - Confocal imaging
  - DiI labeling
  - Quantitative PCR (qPCR)
  - Single-cell RNA-seq
  - Sequence alignment and preprocessing
  - PCA and tSNE
  - Iterative Clustering for Identifying Markers (ICIM)
  - Overdispersion analysis and differential expression analysis
  - Cluster map in Figure 1
  - Cell type coverage in the antenna
  - Transcription factor (TF) gene lists
- QUANTIFICATION AND STATISTICAL ANALYSIS
- DATA AND CODE AVAILABILITY

SUPPLEMENTAL INFORMATION

Supplemental Information can be found online at https://doi.org/10.1016/j.cub.2020.01.049.

ACKNOWLEDGMENTS

We thank H. Bellen, L. Zipursky, I. Grunwald Kadow, J. Simpson, the Bloomington *Drosophila* Stock Center, and the Vienna *Drosophila* Resource Center for reagents; J. Lui and E. Richman for discussions; N. Neff, J. Okamoto, and Chan-Zuckerberg Biohub for assistance with sequencing; Y. Ge for assistance on fly work; and A. Shuster, J. Lui, and D. Pederick for comments on the manuscript. H.L. was a Stanford Neuroscience Institute interdisciplinary postdoctoral scholar. F.H. acknowledges support from the National Science Foundation Graduate Research Fellowship. J.L. acknowledges Genentech Foundation Predoctoral and Vanessa Kong Kerzner Graduate Fellowships. J.M.K. is a Fellow of the Jane Coffin Childs Memorial Fund. S.R.Q. is a Chan Zuckerberg investigator, and L.L. is a Howard Hughes Medical Institute (HHMI) investigator. This work was supported by National Institutes of Health grants 1K99AG062746-01 (to H.L.) and R01-DC005982 (to L.L.).

AUTHOR CONTRIBUTIONS

H.L. and L.L. conceived this project. H.L., T.L., and L.L. designed experiments with support from F.H. and S.R.Q. H.L. and T.L collected samples and

(F) Quantification for the receptor expression in three *unpg*+ ORN types and four *unpg*− ones.
(G) In *unpg-RNAi* flies, *Gr21a* expression is lost consistently, and *Gr63a*+ axons show stereotyped mistargeting (arrowheads). Quantifications are shown on the right.
(H) Schematic illustrating the strategy of DiI labeling for four ORN types from the same ab1 sensilla in the antenna: *Or42b* and *Or10a* (*unpg*−) as well as *Gr21a* and *Or92a* (*unpg*+).
(I) For DiI labeling, *Gr63a-syt:GFP* is used to monitor V-ORNs. In WT flies, DiI labels VA2 in an anterior section of the antennal lobe and DM1, DL1, and V in a posterior section. In *unpg-RNAi* flies, DiI labels a diffuse area (arrowheads) around VA2 in the anterior section, labels DL1 and DM1 normally, and co-labels *Gr63a*-posistive V-ORNs, which show mistargeting phenotypes. Schematic on the right summarizes DiI labeling in WT and *unpg-RNAi* flies. Quantifications are shown on the right; antennal lobe numbers (n) are also indicated.
(J) Summary of the regulation of olfactory receptor expression and wiring in V-ORNs by TFs *fkh* and *unpg*.
D, dorsal; L, lateral; WT, wild type. Scale bars, 20 μm. See also Figure S5.

performed scRNA-seq. H.L. analyzed data with help from F.H., S.S.K., R.C.J., and J.M.K. T.L. performed DiI labeling experiments, and H.L. performed all other fly experiments with help from T.L., J.L., Q.X., C.X., B.W., C.N.M., D.V., A.X., and D.J.L. Q.X. performed qRT-PCR. H.L. and L.L. wrote the paper with input from T.L., F.H., and S.R.Q.

DECLARATION OF INTERESTS

The authors declare no competing interests.

Received: December 12, 2019
Revised: January 10, 2020
Accepted: January 14, 2020
Published: February 13, 2020

REFERENCES

1. Sanes, J.R., and Zipursky, S.L. (2010). Design principles of insect and vertebrate visual systems. Neuron *66*, 15–36.
2. Kolodkin, A.L., and Tessier-Lavigne, M. (2011). Mechanisms and molecules of neuronal wiring: a primer. Cold Spring Harb. Perspect. Biol. *3*, a001727.
3. Dalton, R.P., and Lomvardas, S. (2015). Chemosensory receptor specificity and regulation. Annu. Rev. Neurosci. *38*, 331–349.
4. Li, H., Shuster, S.A., Li, J., and Luo, L. (2018). Linking neuronal lineage and wiring specificity. Neural Dev. *13*, 5.
5. Clyne, P.J., Warr, C.G., Freeman, M.R., Lessing, D., Kim, J., and Carlson, J.R. (1999). A novel family of divergent seven-transmembrane proteins: candidate odorant receptors in *Drosophila*. Neuron *22*, 327–338.
6. Gao, Q., and Chess, A. (1999). Identification of candidate *Drosophila* olfactory receptors from genomic DNA sequence. Genomics *60*, 31–39.
7. Vosshall, L.B., Amrein, H., Morozov, P.S., Rzhetsky, A., and Axel, R. (1999). A spatial map of olfactory receptor expression in the *Drosophila* antenna. Cell *96*, 725–736.
8. Vosshall, L.B., and Stocker, R.F. (2007). Molecular architecture of smell and taste in *Drosophila*. Annu. Rev. Neurosci. *30*, 505–533.
9. Wilson, R.I. (2013). Early olfactory processing in *Drosophila*: mechanisms and principles. Annu. Rev. Neurosci. *36*, 217–241.
10. Axel, R. (1995). The molecular logic of smell. Sci. Am. *273*, 154–159.
11. Feinstein, P., Bozza, T., Rodriguez, I., Vassalli, A., and Mombaerts, P. (2004). Axon guidance of mouse olfactory sensory neurons by odorant receptors and the beta2 adrenergic receptor. Cell *117*, 833–846.
12. Wang, F., Nemes, A., Mendelsohn, M., and Axel, R. (1998). Odorant receptors govern the formation of a precise topographic map. Cell *93*, 47–60.
13. Imai, T., Suzuki, M., and Sakano, H. (2006). Odorant receptor-derived cAMP signals direct axonal targeting. Science *314*, 657–661.
14. Elmore, T., and Smith, D.P. (2001). Putative *Drosophila* odor receptor OR43b localizes to dendrites of olfactory neurons. Insect Biochem. Mol. Biol. *31*, 791–798.
15. Darmanis, S., Sloan, S.A., Zhang, Y., Enge, M., Caneda, C., Shuer, L.M., Hayden Gephart, M.G., Barres, B.A., and Quake, S.R. (2015). A survey of human brain transcriptome diversity at the single cell level. Proc. Natl. Acad. Sci. USA *112*, 7285–7290.
16. Hanchate, N.K., Kondoh, K., Lu, Z., Kuang, D., Ye, X., Qiu, X., Pachter, L., Trapnell, C., and Buck, L.B. (2015). Single-cell transcriptomics reveals receptor transformations during olfactory neurogenesis. Science *350*, 1251–1255.
17. Shekhar, K., Lapan, S.W., Whitney, I.E., Tran, N.M., Macosko, E.Z., Kowalczyk, M., Adiconis, X., Levin, J.Z., Nemesh, J., Goldman, M., et al. (2016). Comprehensive classification of retinal bipolar neurons by single-cell transcriptomics. Cell *166*, 1308–1323.e30.
18. Tasic, B., Menon, V., Nguyen, T.N., Kim, T.K., Jarsky, T., Yao, Z., Levi, B., Gray, L.T., Sorensen, S.A., Dolbeare, T., et al. (2016). Adult mouse cortical cell taxonomy revealed by single cell transcriptomics. Nat. Neurosci. *19*, 335–346.
19. Li, H., Horns, F., Wu, B., Xie, Q., Li, J., Li, T., Luginbuhl, D.J., Quake, S.R., and Luo, L. (2017). Classifying *Drosophila* olfactory projection neuron subtypes by single-cell RNA sequencing. Cell *171*, 1206–1220.e22.
20. Zeisel, A., Hochgerner, H., Lönnerberg, P., Johnsson, A., Memic, F., van der Zwan, J., Häring, M., Braun, E., Borm, L.E., La Manno, G., et al. (2018). Molecular architecture of the mouse nervous system. Cell *174*, 999–1014.e22.
21. Saunders, A., Macosko, E.Z., Wysoker, A., Goldman, M., Krienen, F.M., de Rivera, H., Bien, E., Baum, M., Bortolin, L., Wang, S., et al. (2018). Molecular diversity and specializations among the cells of the adult mouse brain. Cell *174*, 1015–1030.e16.
22. Jefferis, G.S.X.E., Vyas, R.M., Berdnik, D., Ramaekers, A., Stocker, R.F., Tanaka, N.K., Ito, K., and Luo, L. (2004). Developmental origin of wiring specificity in the olfactory system of *Drosophila*. Development *131*, 117–130.
23. Picelli, S., Faridani, O.R., Björklund, A.K., Winberg, G., Sagasser, S., and Sandberg, R. (2014). Full-length RNA-seq from single cells using Smart-seq2. Nat. Protoc. *9*, 171–181.
24. Campello, R.J.G.B., Moulavi, D., Zimek, A., and Sander, J. (2013). A framework for semi-supervised and unsupervised optimal extraction of clusters from hierarchies. Data Min. Knowl. Discov. *27*, 344–371.
25. Lee, P.-T., Zirin, J., Kanca, O., Lin, W.-W., Schulze, K.L., Li-Kroeger, D., Tao, R., Devereaux, C., Hu, Y., Chung, V., et al. (2018). A gene-specific *T2A-GAL4* library for *Drosophila*. eLife *7*, e35574.
26. Endo, K., Aoki, T., Yoda, Y., Kimura, K., and Hama, C. (2007). Notch signal organizes the *Drosophila* olfactory circuitry by diversifying the sensory neuronal lineages. Nat. Neurosci. *10*, 153–160.
27. Jenett, A., Rubin, G.M., Ngo, T.-T.B., Shepherd, D., Murphy, C., Dionne, H., Pfeiffer, B.D., Cavallaro, A., Hall, D., Jeter, J., et al. (2012). A GAL4-driver line resource for *Drosophila* neurobiology. Cell Rep. *2*, 991–1001.
28. Stockinger, P., Kvitsiani, D., Rotkopf, S., Tirián, L., and Dickson, B.J. (2005). Neural circuitry that governs *Drosophila* male courtship behavior. Cell *121*, 795–807.
29. Couto, A., Alenius, M., and Dickson, B.J. (2005). Molecular, anatomical, and functional organization of the *Drosophila* olfactory system. Curr. Biol. *15*, 1535–1547.
30. Fishilevich, E., and Vosshall, L.B. (2005). Genetic and functional subdivision of the *Drosophila* antennal lobe. Curr. Biol. *15*, 1548–1553.
31. Silbering, A.F., Rytz, R., Grosjean, Y., Abuin, L., Ramdya, P., Jefferis, G.S.X.E., and Benton, R. (2011). Complementary function and integrated wiring of the evolutionarily distinct *Drosophila* olfactory subsystems. J. Neurosci. *31*, 13357–13375.
32. Scott, K., Brady, R., Jr., Cravchik, A., Morozov, P., Rzhetsky, A., Zuker, C., and Axel, R. (2001). A chemosensory gene family encoding candidate gustatory and olfactory receptors in *Drosophila*. Cell *104*, 661–673.
33. Benton, R., Vannice, K.S., Gomez-Diaz, C., and Vosshall, L.B. (2009). Variant ionotropic glutamate receptors as chemosensory receptors in *Drosophila*. Cell *136*, 149–162.
34. Larsson, M.C., Domingos, A.I., Jones, W.D., Chiappe, M.E., Amrein, H., and Vosshall, L.B. (2004). *Or83b* encodes a broadly expressed odorant receptor essential for *Drosophila* olfaction. Neuron *43*, 703–714.
35. Ghaemmaghami, S., Huh, W.-K., Bower, K., Howson, R.W., Belle, A., Dephoure, N., O'Shea, E.K., and Weissman, J.S. (2003). Global analysis of protein expression in yeast. Nature *425*, 737–741.
36. Pfreundt, U., James, D.P., Tweedie, S., Wilson, D., Teichmann, S.A., and Adryan, B. (2010). FlyTF: improved annotation and enhanced functionality of the *Drosophila* transcription factor database. Nucleic Acids Res. *38*, D443–D447.
37. Clyne, P.J., Certel, S.J., de Bruyne, M., Zaslavsky, L., Johnson, W.A., and Carlson, J.R. (1999). The odor specificities of a subset of olfactory receptor neurons are governed by Acj6, a POU-domain transcription factor. Neuron *22*, 339–347.

38. Komiyama, T., Carlson, J.R., and Luo, L. (2004). Olfactory receptor neuron axon targeting: intrinsic transcriptional control and hierarchical interactions. Nat. Neurosci. *7*, 819–825.
39. Tichy, A.L., Ray, A., and Carlson, J.R. (2008). A new *Drosophila* POU gene, *pdm3*, acts in odor receptor expression and axon targeting of olfactory neurons. J. Neurosci. *28*, 7121–7129.
40. Bai, L., and Carlson, J.R. (2010). Distinct functions of acj6 splice forms in odor receptor gene choice. J. Neurosci. *30*, 5028–5036.
41. Jafari, S., Alkhori, L., Schleiffer, A., Brochtrup, A., Hummel, T., and Alenius, M. (2012). Combinatorial activation and repression by seven transcription factors specify *Drosophila* odorant receptor expression. PLoS Biol. *10*, e1001280.
42. Lee, T., and Luo, L. (1999). Mosaic analysis with a repressible cell marker for studies of gene function in neuronal morphogenesis. Neuron *22*, 451–461.
43. Jones, W.D., Cayirlioglu, P., Kadow, I.G., and Vosshall, L.B. (2007). Two chemosensory receptors together mediate carbon dioxide detection in *Drosophila*. Nature *445*, 86–90.
44. Kwon, J.Y., Dahanukar, A., Weiss, L.A., and Carlson, J.R. (2007). The molecular basis of CO_2 reception in *Drosophila*. Proc. Natl. Acad. Sci. USA *104*, 3574–3578.
45. Weigel, D., Jürgens, G., Küttner, F., Seifert, E., and Jäckle, H. (1989). The homeotic gene *fork head* encodes a nuclear protein and is expressed in the terminal regions of the Drosophila embryo. Cell *57*, 645–658.
46. Chiang, C., Young, K.E., and Beachy, P.A. (1995). Control of Drosophila tracheal branching by the novel homeodomain gene unplugged, a regulatory target for genes of the bithorax complex. Development *121*, 3901–3912.
47. Cui, X., and Doe, C.Q. (1995). The role of the cell cycle and cytokinesis in regulating neuroblast sublineage gene expression in the Drosophila CNS. Development *121*, 3233–3243.
48. Hong, W., and Luo, L. (2014). Genetic control of wiring specificity in the fly olfactory system. Genetics *196*, 17–29.
49. Hong, W., Mosca, T.J., and Luo, L. (2012). Teneurins instruct synaptic partner matching in an olfactory map. Nature *484*, 201–207.
50. Ward, A., Hong, W., Favaloro, V., and Luo, L. (2015). Toll receptors instruct axon and dendrite targeting and participate in synaptic partner matching in a *Drosophila* olfactory circuit. Neuron *85*, 1013–1028.
51. Ni, L., Bronk, P., Chang, E.C., Lowell, A.M., Flam, J.O., Panzano, V.C., Theobald, D.L., Griffith, L.C., and Garrity, P.A. (2013). A gustatory receptor paralogue controls rapid warmth avoidance in *Drosophila*. Nature *500*, 580–584.
52. Enjin, A., Zaharieva, E.E., Frank, D.D., Mansourian, S., Suh, G.S.B., Gallio, M., and Stensmyr, M.C. (2016). Humidity sensing in *Drosophila*. Curr. Biol. *26*, 1352–1358.
53. Budelli, G., Ni, L., Berciu, C., van Giesen, L., Knecht, Z.A., Chang, E.C., Kaminski, B., Silbering, A.F., Samuel, A., Klein, M., et al. (2019). Ionotropic receptors specify the morphogenesis of phasic sensors controlling rapid thermal preference in *Drosophila*. Neuron *101*, 738–747.e3.
54. Knecht, Z.A., Silbering, A.F., Cruz, J., Yang, L., Croset, V., Benton, R., and Garrity, P.A. (2017). Ionotropic receptor-dependent moist and dry cells control hygrosensation in *Drosophila*. eLife *6*, e26654.
55. Morey, M., Yee, S.K., Herman, T., Nern, A., Blanco, E., and Zipursky, S.L. (2008). Coordinate control of synaptic-layer specificity and rhodopsins in photoreceptor neurons. Nature *456*, 795–799.
56. Courgeon, M., and Desplan, C. (2019). Coordination between stochastic and deterministic specification in the *Drosophila* visual system. Science *366*, eaay6727.
57. Xie, Q., Wu, B., Li, J., Xu, C., Li, H., Luginbuhl, D.J., Wang, X., Ward, A., and Luo, L. (2019). Transsynaptic Fish-lips signaling prevents misconnections between nonsynaptic partner olfactory neurons. Proc. Natl. Acad. Sci. USA *116*, 16068–16073.
58. Sweeney, L.B., Couto, A., Chou, Y.-H., Berdnik, D., Dickson, B.J., Luo, L., and Komiyama, T. (2007). Temporal target restriction of olfactory receptor neurons by Semaphorin-1a/PlexinA-mediated axon-axon interactions. Neuron *53*, 185–200.
59. Potter, C.J., Tasic, B., Russler, E.V., Liang, L., and Luo, L. (2010). The Q system: a repressible binary system for transgene expression, lineage tracing, and mosaic analysis. Cell *141*, 536–548.
60. Chotard, C., Leung, W., and Salecker, I. (2005). *glial cells missing* and *gcm2* cell autonomously regulate both glial and neuronal development in the visual system of *Drosophila*. Neuron *48*, 237–251.
61. Li, J., Guajardo, R., Xu, C., Wu, B., Li, H., Li, T., Luginbuhl, D.J., Xie, X., and Luo, L. (2018). Stepwise wiring of the *Drosophila* olfactory map requires specific Plexin B levels. eLife *7*, e39088.
62. Zhu, H., and Luo, L. (2004). Diverse functions of N-cadherin in dendritic and axonal terminal arborization of olfactory projection neurons. Neuron *42*, 63–75.
63. Wu, J.S., and Luo, L. (2006). A protocol for dissecting *Drosophila melanogaster* brains for live imaging or immunostaining. Nat. Protoc. *1*, 2110–2115.
64. Komiyama, T., Johnson, W.A., Luo, L., and Jefferis, G.S.X.E. (2003). From lineage to wiring specificity. POU domain transcription factors control precise connections of *Drosophila* olfactory projection neurons. Cell *112*, 157–167.
65. Dobin, A., Davis, C.A., Schlesinger, F., Drenkow, J., Zaleski, C., Jha, S., Batut, P., Chaisson, M., and Gingeras, T.R. (2013). STAR: ultrafast universal RNA-seq aligner. Bioinformatics *29*, 15–21.
66. Anders, S., Pyl, P.T., and Huber, W. (2015). HTSeq–a Python framework to work with high-throughput sequencing data. Bioinformatics *31*, 166–169.
67. van der Maaten, L., and Hinton, G. (2008). Visualizing data using t-SNE. J. Mach. Learn. Res. *9*, 2579–2605.

STAR★METHODS

KEY RESOURCES TABLE

REAGENT or RESOURCE	SOURCE	IDENTIFIER
Antibodies		
Rat anti-DNcad	Developmental Studies Hybridoma Bank	DN-Ex #8
Chicken anti-GFP	Aves Labs	GFP-1020
Rabbit anti-DsRed	Clontech	632496
Rat anti-ratCD2	AbD Serotec	OX-34
Deposited Data		
Sequencing reads	This paper	GSE143038
Preprocessed sequence data	This paper	GSE143038
Experimental Models: Organisms/Strains		
D. melanogaster: *nSyb-GAL4*	Bloomington *Drosophila* Stock Center	BDSC: 51635
D. melanogaster: *act5C-GAL4*	Bloomington *Drosophila* Stock Center	BDSC: 3954
D. melanogaster: *NompB-T2A-GAL4*	Bloomington *Drosophila* Stock Center	BDSC: 76632
D. melanogaster: *5-HT1B-T2A-GAL4*	Bloomington *Drosophila* Stock Center	BDSC: 76668
D. melanogaster: *UAS-STOP-mCD8GFP*	[49]	BDSC: 41573
D. melanogaster: *DIP-epsilon-T2A-GAL4*	[27]	BDSC: 67502
D. melanogaster: *unpg-RNAi*	Vienna *Drosophila* Resource Center	VDRC #107638
D. melanogaster: *AM29-GAL4*	[26]	N/A
D. melanogaster: *GMR86C10-GAL4*	[57]	N/A
D. melanogaster: *GMR85A10-GAL4*	[27]	N/A
D. melanogaster: *peb-GAL4*	[58]	N/A
D. melanogaster: *GH146-Flp*	[59]	N/A
D. melanogaster: *ey-Flp*	[60]	N/A
D. melanogaster: *Or85f-GAL4*	[29]	N/A
D. melanogaster: *Or42b-mCD8:GFP*	[29]	N/A
D. melanogaster: *Or67a-mCD8:GFP*	[29]	N/A
D. melanogaster: *Or98a-mCD8:GFP*	[29]	N/A
D. melanogaster: *Or92a-rCD2*	[61]	N/A
D. melanogaster: *Or47b-rCD2*	[62]	N/A
D. melanogaster: *Or88a-mtdT*	[50]	N/A
D. melanogaster: *Or10a-LexA*	[30]	N/A
D. melanogaster: *Gr21a-syt:GFP*	[43]	N/A
D. melanogaster: *Gr63a-syt:GFP*	[43]	N/A
D. melanogaster: GMR86C10-LexA	This paper	N/A
Oligonucleotides		
Actin5C (qPCR forward primer): 5′-CTCGCCACTTGCGTTTACAGT-3′	This paper	N/A
Actin5C (qPCR reverse primer): 5′-TCCATATCGTCCCAGTTGGTC-3′	This paper	N/A
unpg (qPCR forward primer 1F): 5′- CTACAACGGCGAGATGGACA –3′	This paper	N/A
unpg (qPCR reverse primer 1R): 5′- TTGGAGTTTGAGCTGGAGCC –3′	This paper	N/A

(*Continued on next page*)

Continued		
REAGENT or RESOURCE	SOURCE	IDENTIFIER
unpg (qPCR forward primer 2F): 5′- GGAACTACAACGGCGAGATG −3′	This paper	N/A
unpg (qPCR reverse primer 2R): 5′- GATACTTCTTGGCGTGGAACT −3′	This paper	N/A
Software and Algorithms		
Iterative Clustering for Identifying Markers (ICIM)	[19]	https://github.com/felixhorns/FlyPN

LEAD CONTACT AND MATERIALS AVAILABILITY

Further information and requests for resources and reagents should be directed to and will be fulfilled by the lead contact, Liqun Luo (lluo@stanford.edu). This study did not generate new unique reagents.

EXPERIMENTAL MODEL AND SUBJECT DETAILS

Fly stocks

The following fly lines were used in this study. *nSyb-GAL4* (Bloomington *Drosophila* Stock Center, BDSC #51635); *act5C-GAL4* (BDSC #3954); *AM29-GAL4* [26]; *GMR86C10-GAL4* [57] and *GMR85A10-GAL4* [27]; *NompB-T2A-GAL4* (BDSC #76632); *DIP-epsilon-T2A-GAL4* (BDSC #67502); *5-HT1B-T2A-GAL4* (BDSC #76668); *tsh-T2A-GAL4* [25]; *acj6*^{6} [37]; *Mz19-QF* [49]; *fkh-RNAi (*BDSC #33760, #58059*); UAS-Robo2 (*BDSC #66886); *Robo2-RNAi (*BDSC #9286), *unpg-RNAi* (VDRC #107638); *peb-GAL4* [58]; *GH146-Flp* [59]; *ey-Flp* [60]; *UAS-STOP-mCD8:GFP* [49]; *Or-GAL4* and *Or-mCD8:GFP* [29]; *Or85f-GAL4, Or42b-mCD8:GFP, Or67a-mCD8:GFP, Or98a-mCD8:GFP; Or92a-rCD2* [61]; *Or47b-rCD2* [62]; *Or88a-mtdT* [50]; *Or10a-LexA* [30]; *Gr21a-syt:GFP* and *Gr63a-syt:GFP* [43].

METHOD DETAILS

Immunostaining

Tissue dissection and immunostaining were performed following previously described methods [63]. Briefly, fly pupal and adult brains were dissected in 1x PBS and then fixed in 4% paraformaldehyde (20% paraformaldehyde diluted in PBS with 0.015% Triton X-100) for 20 min at room temperature. Fixed brains were washed three times with PBST (PBS with 0.3% Triton X-100) and incubated in PBST twice for 20 min. The samples were incubated in blocking buffer (5% normal goat serum in PBST) for 30 min at room temperature or overnight at 4°C. Then, primary antibodies diluted in blocking buffer were applied and samples were incubated for 24–48 h at 4°C. Then, samples were washed using PBST for 20 min twice, and secondary antibodies diluted in blocking buffer were applied and samples were incubated in dark for more than 24 h at 4°C. Samples were washed in PBST for 20 min twice and mounting solution (Slow Fade Gold) was added. Samples were left in mounting solution for at least 1 h before mounting them onto glass slides. All wash steps were performed at room temperature. Primary antibodies used in this study include rat anti-DNcad (DN-Ex #8; 1:40; DSHB), chicken anti-GFP (1:1000; Aves Labs), rabbit anti-DsRed (1:250; Clontech), mouse anti-ratCD2 (OX-34; 1:200; AbD Serotec). Secondary antibodies were raised in goat or donkey against rabbit, mouse, rat, and chicken antisera (Jackson Immunoresearch), conjugated to Alexa 405, 488, FITC, Cy3, Cy5, or Alexa 647.

MARCM analysis

For ORN MARCM clonal analysis, *Tub-GAL80,hsFlp,FRT19A;AM29-GAL4* flies were crossed either with *UAS-mCD8:GFP,FRT19A* (control) or with *acj6*^{6}*,UAS- mCD8:GFP,FRT19A.* Newly formed pupae (0–2hAPF) were heat-shocked for 1 hour at 37°C and adult flies were dissected for axon projection analysis. While *acj6* is required for dendrite targeting of a subset of PNs [64] and PN targeting can affect ORN axon targeting [50], the observed ORN axon targeting phenotype is not due to loss of *acj6* in unlabeled PN clones because all PNs are born before the pupal stage and therefore could not produce clones under our heat-shock condition.

Confocal imaging

All confocal images were taken through a Z stack scan from most anterior to the most posterior of the antenna or antennal lobe using the Zeiss LSM 780 system. Then images were processed with ImageJ and Adobe Illustrator. For quantification in Figures 4 and 5, at least 10 flies (20 antennal lobes) were used.

DiI labeling

DiI (Sigma 468495) in saturated DMSO solution was applied to the medioproximal corner of the third antennal segment of adult flies, where the ab1 sensilla are located, through glass micropipette using a micromanipulator. Flies were recovered for 24h after labeling

before their brains were dissected, mounted in 30% sucrose, and imaged using a confocal microscope. Mistargeting phenotypes of both antennal lobes from each fly were quantified in WT control and *unpg-RNAi* expressing flies. Since 4 types of ORNs are localized in ab1 sensilla, we only focused on flies that are labeled for 4 glomeruli. Out of 11 WT flies, 1 was labeled for many glomeruli, which is likely due to labeling of additional sensilla near ab1 during DiI application. 3 out of 14 *unpg-RNAi* expressing flies showed similar additional labeling and were excluded from quantification. In total, 10 WT and 11 *unpg-RNAi* flies (20 and 22 antennal lobes) were quantified for VA2 ORN axon targeting.

Quantitative PCR (qPCR)

Total RNA was extracted using MiniPrep kit (Zymo Research, R1054) from either *actin5C-GAL4, w*^{1118} (control) or *actin5C-GAL4; unpg-RNAi* flies at middle pupal stage (N = 3 replicates for each condition; 5 pupae per replicate). cDNA was synthesized using an oligo-dT primer. qPCR was performed on a Bio-Rad CFX96 detection system. *p-value* was calculated using Student's t test. Relative expression was normalized to *actin5C*. Primer sequences used for qPCR were:

actin5C (F): 5′-CTCGCCACTTGCGTTTACAGT-3′
actin5C (R): 5′-TCCATATCGTCCCAGTTGGTC-3′
unpg pair 1 (F): 5′- CTACAACGGCGAGATGGACA-3′
unpg pair 1 (R): 5′- TTGGAGTTTGAGCTGGAGCC-3′
unpg pair 2 (F): 5′- GGAACTACAACGGCGAGATG-3′
unpg pair 2 (R): 5′- GATACTTCTTGGCGTGGAACT C-3′

Single-cell RNA-seq

Single-cell RNA-seq was performed following the protocol that we developed recently [19]. Briefly, *Drosophila* third antennal segments with mCD8:GFP-labeled cells using specific GAL4 drivers were manually dissected. Single-cell suspensions were then prepared. Single labeled cells were sorted via Fluorescence Activated Cell Sorting (FACS) into individual wells of 96-well plates containing lysis buffer using an SH800 instrument (Sony Biotechnology). Full-length poly(A)-tailed RNA was reverse-transcribed and amplified by PCR following the SMART-seq2 protocol[47] with several modifications as below. To increase cDNA yield and detection efficiency, we increased the number of PCR cycles to 25. To reduce the amount of primer dimer PCR artifacts, we digested the reverse-transcribed first-strand cDNA using lambda exonuclease (New England Biolabs) (37°C for 30 min) prior to PCR amplification. Sequencing libraries were prepared from amplified cDNA using tagmentation (Nextera XT). Sequencing was performed using the Illumina Nextseq 500 platform with paired-end 75 bp reads.

Sequence alignment and preprocessing

Reads were aligned to the *Drosophila melanogaster* genome (r6.10) using STAR (2.4.2a) [65] with the ENCODE standard options, except "–outFilterScoreMinOverLread 0.4–outFilterMatchNminOverLread 0.4–outFilterMismatchNmax 999–outFilterMismatchNoverLmax 0.04." Uniquely mapped reads that overlap with genes were counted using HTSeq-count (0.7.1) [66] with default settings except "-m intersection-strict." Cells having fewer than 100,000 uniquely mapped reads were removed. To normalize for differences in sequencing depth across individual cells, we rescaled gene counts to counts per million (CPM). All analyses were performed after converting gene counts to logarithmic space via the transformation Log_2(CPM+1). Sequenced cells were filtered for expression of canonical neuronal genes (*elav, brp, Syt1, nSyb, CadN,* and *mCD8GFP*), retaining only those cells that expressed at least 4/6 genes at Log_2 (CPM+1) $\geq$ 3.

PCA and tSNE

Principal component analysis (PCA) and t-distributed Stochastic Neighbor Embedding (tSNE) were used for visualizing *Drosophila* scRNA-seq data as detailed previously [19]. Briefly, to visualize and interpret high dimensional gene expression data, we obtained two-dimensional projections of the cell population by first reducing the dimensionality of the gene expression matrix using PCA, then further reducing the dimensionality of these components using tSNE [67]. We performed PCA for Figure 1D on a reduced gene expression matrix composed of the top 500 overdispersed genes. The top 8 principal components (8 PCs) were used. We further reduced these components using tSNE to project them into a two-dimensional space.

Iterative Clustering for Identifying Markers (ICIM)

We previously developed an unsupervised machine learning algorithm called ICIM to identify genes that distinguish transcriptome clusters for different fly olfactory projection neuron (PN) subtypes [19] (available at https://github.com/felixhorns/FlyPN). We performed similar analysis for ORNs with several modifications of the adjustable parameters, including pearson correlation and dropout threshold, and identified 408 ICIM genes, which we used for further dimensionality reduction by PCA. The top 18 PCs were further reduced to two dimensions using tSNE. HDBSCAN, a hierarchical density-based unbiased clustering algorithm [24], was used to identify clusters.

We observed that standard dimensionality reduction and clustering methods using PCA and tSNE failed to discriminate subpopulations that corresponded to known lineages and molecular features of PNs [19] or ORNs (current study). We attributed the failure of

these methods to the high degree of similarity of transcriptional states among olfactory neuron types, which represent closely-related neurons having similar functions. Thus, olfactory neuron types may be distinguished by a small number of genes. We developed ICIM as a strategy to identify the most informative genes for distinguishing subpopulations within a population of closely-related cells in an unbiased way.

Briefly, starting with a population of cells, we first identify the top 100 overdispersed genes. Next, we expand this set of genes by finding genes whose expression profiles are strongly correlated. We also filter this set of genes by (1) removing those having < 2 correlated partners to remove noisy genes, and (2) those that are expressed in > 80% of cells to remove housekeeping genes. Cells are then clustered. We cut the dendrogram at the deepest branch and partition the population into two subpopulations. The same steps are then performed iteratively on each subpopulation. Iteration continues until a population cannot be split. The termination condition is defined as the minimum terminal branch length being larger than 0.2. The result of this analysis is a set of genes that discriminate subpopulations within a population, which can be used for dimensionality reduction.

Overdispersion analysis and differential expression analysis

Overdispersion analysis and differential expression analysis were previously described [19]. Briefly, genes that are highly variable within a population often carry important information for distinguishing cell types. Variability of gene expression depends strongly on the mean expression level of a gene. This motivates the use of a metric called dispersion, which measures the variability of a gene's expression level in comparison with other genes that are expressed at a similar level. Overdispersed genes are those that display higher variability than expected based on their mean expression level. To identify overdispersed genes, we binned genes into 20 bins based on their mean expression across all cells. We then calculated a log-transformed Fano factor D(x) of each gene x

$$D(x) = \log_{10}\left[\sigma^2(x) \,/\, \mu(x)\right]$$

where $\sigma^2(x)$ is the variance and $\mu(x)$ is the mean of the expression level of the gene across cells. Finally, we calculated the dispersion d(x) as the Z-score of the Fano factor within its bin

$$d(x) = D(x) - \text{Mean}[D(x)] / \text{Std}[D(x)]$$

where Mean[D(x)] is the mean log-transformed Fano factor within the bin and Std[D(x)] is the standard deviation of the log-transformed Fano factor within the bin. We then rank genes by their dispersion and select the top genes for downstream analysis.

To find differentially expressed genes, we used the Mann-Whitney U test, a non-parametric test that detects differences in the level of gene expression between two populations. The Mann-Whitney U test is advantageous for this application because it makes very general assumptions: (1) observations from both groups are independent and (2) the gene expression levels are ordinal (i.e., can be ranked). Thus the test applies to distributions of gene expression levels across cells, which rarely follow a normal distribution. Using the Mann-Whitney U test, we compared the distributions of expression levels of every gene separately. P values were adjusted using the Bonferroni correction for multiple testing. Different significance thresholds for determining whether a gene is differentially expressed were used for various analyses in this work.

Cluster map in Figure 1

In Figure 1B, we used all ORNs for the tSNE plot, including *AM29-GAL4+* and *85A10-GAL4+*, 2 and 5 ORN types, that are used to decode cluster identities later. This is because for tSNE plots, each time when we add new cells, the overall cluster layout (e.g., the relative positions of clusters) is changed, which may cause confusion to the general readership. To avoid such confusion, we decided to plot all cells (including 2 and 5 types) in Figure 1B, so that the cluster map will remain the same as in Figure 2, which we used to decode cluster identities.

Cell type coverage in the antenna

We have analyzed 1016 ORNs, which are from 44 ORN types. We classified cells into clusters in an unbiased manner using HDBSCAN with min_cluster_size = 6 and min_samples = 6 on coordinates after tSNE projection; under these condtions, each cluster requires a minimum of 6 cells. This resulted in 33 clusters. It is likely that, for certain ORN types, we covered fewer than 6 cells, which were not enough to form a cluster. This is also consistent with our observation that when we project our *AM29-GAL4* cells into the pan-neuronal *nSyb-GAL4*-based reference dataset, the accuracy is very low (data not shown). This can explain why cluster #3 (Figure 2H) contains mostly *AM29-GAL4* cells, with very few *nSyb-GAL4* cells.

Transcription factor (TF) gene lists

To identify genes that are transcription factors (TFs), we used manually curated lists. We obtained a list of *Drosophila* TFs from the FlyTF v1 database (Database: http://www.mrc-lmb.cam.ac.uk/genomes/FlyTF). These lists were manually curated to remove spurious annotations and redundancies according to Flybase annotation, resulting in 1045 TFs (see https://github.com/felixhorns/FlyPN), which were used for analysis in Figure 3 and S4A. For Figure 3, we tested several levels of thresholds that define a positive cell and obtained similar results. For example, similar total numbers (915, 899, and 890) of detected TFs in at least one cell were obtained when using three different thresholds, $\text{Log}_2(\text{CPM}+1) \geq 2$, 3, or 4.

QUANTIFICATION AND STATISTICAL ANALYSIS

All RNA-seq data analysis was performed in Python using Numpy, Scipy, Pandas, scikit-learn, and a custom single-cell RNA-seq module. We used the Mann-Whitney U test to find differentialy expressed genes between two cell populations. For phenotype quantification in Figure 4 and 5, Student's t test was used.

DATA AND CODE AVAILABILITY

Sequencing reads and preprocessed data are available from NCBI Gene Expression Omnibus (GSE143038). Python codes for figures are available from Github (https://github.com/Hongjie-Li/FlyORN).